



Influence of Cationic and Nonionic Surfactant-Modified Zn-Co/TiO₂ LDHs for the Removal of Organic Pollutant

Amira A. Hashem^{*,*}, Walaa R. Abd-Ellatif^a, Nouran G. Mahmoud^a, Maha K. El-Aiashy^a,
Essam M. Ezzo^a, Sawsan A. Mahmoud^b



^a Faculty of Women for Art, Science and Education, Ain Shams University, Asma Fahmy Street, Heliopolis 11757, Cairo, Egypt

^b Processes Development Department, Egyptian Petroleum Research Institute, P.O.Box: 11727, Cairo, Egypt

Abstract

The Nanoparticles of Zinc cobalt LDH with phosphated mesoporous titanium dioxide were prepared by precipitation method and investigated as efficient photocatalysts for anionic E124 dye degradation. Some surfactants were doped for the prepared solids for improvement of its catalytic degradation on which the photodegradation showed dye removal % reached to 100 % with adding surfactant by indirect method. Composite materials were characterized with several methods including X-ray diffraction, Raman spectroscopy, AFM and TEM, which revealed that as an application, photocatalytic degradation of anionic dye was investigated.

Keyword: Ternary layered double hydroxides; Photocatalytic degradation of E124; Nanoparticles; kinetics.

1. Introduction

Most research has been conducted up to find effective photocatalysts. Titanium dioxide has been shown to be the most powerful photocatalyst for industrial use with a crystal structure of anatase form. It has been commonly used as a white pigment for paints, cosmetics and foodstuffs, among the most common materials of our daily lives in industry and technology. TiO₂ has a high chemical stability exposed to acidic and basic compounds, a low cost of non-toxicity, and high oxidation, which allows it to function in many applications [1-6]. A wide range of techniques has been proposed to increase the photo-conversion efficiency of TiO₂ photocatalysts, including metal / non-metal doping, metal loading, hetero-juncting building, and carbon connecting content [7]. Synthetic methods most commonly studied for preparation of ternary Zn-Co/TiO₂ composite particles are deposition of TiO₂ on zinc cobalt oxide surface.

Prepared Zn-Co LDHs composite by co precipitation [8], which showed considerable photocatalytic activity, Trough co precipitation method obtained a ternary of Zn-Co/TiO₂ LDHs and found that the photocatalytic properties of the composite were associated to the crystal shape and the crystal form of TiO₂ loaded on binary composite and the adsorption surface area.

The surfactants have been used as sorbents in many environmental applications and industrial because of their high cation exchange capacity, swelling capacity, high surface area, and resulting strong adsorption-absorption capacities due to the hydration of inorganic cations on the exchange sites [9-11], the clay mineral surface is hydrophilic in nature, which make natural clays ineffective sorbents for adsorbing organic compounds. Surfactant modified composite adsorb the major categories of water contaminants including anions, cations, and organics which treatment of a variety of contaminated waters by addition of other techniques to provide more effective decontamination of polluted water, such as chemical reduction and biological degradation [12-14]. However, for successful application to environmental remediation included the physico-chemical durability to improve the long-term chemical and physical stability.

The main object of this study was to evaluate the effect of different surfactants which consist of a long chain quaternary ammonium ion ($R \geq 12$) such as HDTMA-Cl (hexadecyl trimethyl ammonium) **Fig. 1.** and Triton x-100 **Fig. 2.** on the adsorbing characteristics of surface modified composite.

The sorption of a cationic surfactant (HDTMA-Cl) onto a charged surface involves two major mechanisms ion exchange and hydrophobic interaction due to forming bonding. The parameters governing the interactions between a surfactant molecule and an adsorbent with ion-exchange capability are: (1) the structure of adsorbent, i.e. hydrophobicity or hydrophilicity, surface potential and sign of the surface, ion exchange, porosity, capacity, surface heterogeneity; (2) the structure of adsorbate, i.e. type of surfactant (ionic or non-ionic, aliphatic or aromatic), hydrocarbon chain length (linear or branched), and

*Corresponding author e-mail Amiraabdalla_85@yahoo.co.uk. (Amira abdalla hashem)

Receive Date: 06 April 2024, Revise Date: 09 May 2024, Accept Date: 12 May 2024

DOI: 10.21608/ejchem.2024.281298.9558

©2025 National Information and Documentation Center (NIDOC)

for ionic surfactant, its polar group; and (3) solution conditions (pH, temperature, polarity, dielectric constant, and ionic strength).

2. Experimental

2.1. Materials

Analytical grade chemicals including of titanium tetra isopropoxide (TTIP) was obtained from ADVEN CHEMBIO PVT. LTD Hindi, isopropanol 98% was obtained from Bio.Chem, hexadecyl trimethyl ammonium chloride (HDTMA-Cl) Sigma–Aldrich, Germany, Triton X-100 from Fluka Chemika and phosphoric acid 85% was obtained from Bio.Chem, were used without further purification.

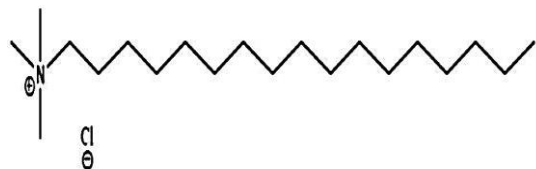


Fig. 1. Structure of surfactant HDTMA-Cl (Hexadecyl trimethyl ammonium chloride)

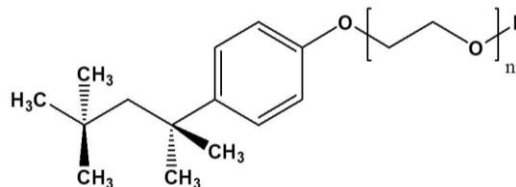


Fig. 2. Structure of the nonionic surfactant Triton X-100 (2-(4-(2,4,4-trimethylpentan-2-yl) phenoxy) ethanol)

2.2. Preparation of the photocatalysts

2.2.1. Phosphated mesoporous titanium dioxide (V)

0.15 mole of titanium tetra isopropoxide, TTIP was dissolved in 150 ml ethanol and then added 13.5 ml of ethylene glycol to the solution. After the vigorously stirring for one hour, 0.015 mol of phosphoric acid was added into the solution. Then the solution was stirred for 30 min till the white powder obtained, then added 100 ml distilled water to obtained white powder which washed with ethanol and water. Finally, Phosphated mesoporous titanium dioxide obtained and dried at 80 °C.

2.2.2. Titanium oxide with zinc cobalt layered double hydroxide composites (XIII–XV)

Sonication-assisted experiments were performed using a sonics vibra-cell (vcx750) sonics processor (max output power 750 Watt at 20 ± 50 kHz) equipped with a modified high-volume continuous flow cell. Core-shell TiO_2 with LDHs, [Zn-Co LDH 1:1) was prepared by co-precipitation in the presence of mesoporous spherical titania particles (~ 200 nm). The insitu precipitation was initiated by sonication for addition of Zn-Co LDH dissolved in isopropanol to suspension of mesoporous TiO_2 dissolved in isopropanol under continuous stirring at room temperature at various speeds between 700–1000 rpm at fixed solution volume and reactor size. The first experiment solutions used for the conventional co-precipitation were mixed at 750Watt ultrasonic agitation for 15 min. In the second experiment, the titanium oxide was sonicated at 750Watt ultrasonic agitation for 15 min. The third experiment was conducted aiming at acceleration of the anion-exchange reaction for LDH with titanium oxide at 750Watt ultrasonic agitation for 15 min. Finally, the product dried at 80 °C for obtained zinc cobalt titanium oxide as shown in **Table 1**.

Moreover, the calcined titanium zinc cobalt oxide was prepared at ratio (0.5-1:1) respectively and then synthesis molar ratios from more active composite by sonication method. In this study, the chemical compositions were optimized, and the reaction active sites were modulated to elucidate the relationship between the structure and the photocatalytic activity.

2.2.2.A. Surface modification of composite through hexadecyl trimethyl ammonium chloride HDTMA-Cl surfactant by indirect method (XVI–XXI)

Surface modification of composite XIV was carried out with supplemental chemicals abreast HDTM-CL. 0.25 g of composite XIV was reacted with 10 mL of 0.05 M of nitric acid and left-over night on the stirrer 300 rpm. Thereafter, 50 mL of 0.5 M sodium bicarbonate was added and allowed to react for 30 min then centrifuged again to remove excess salts. 20 ml of 0.05 M of HDTMA-CL was added and stirred for 6-8 hours at 300 rpm, the slurry was washed to separate any excess salts on the composite. This method used with different concentration of 0.05 M, 0.03 M and 0.01 M of HDTMA-CL surfactant.

2.2.2.B. Surface modification of composite XIV through triton x-100 surfactant by direct method

Surface modification of composite was achieved by adding 0.25 g of composite XIV to a reactor containing 20 ml of surfactant 0.05 M triton X-100 at 300 rpm for 8 hours the magnetic stirrer was maintained to allow for homogenous mixture and then the composite was washed with distilled water to separate any excess salts. Finally, it dried four hours at 80 °C. This method used with surfactant triton X-100.

2.3. Characterization of ternary Zinc-Cobalt-Titanium oxide LDHs Nanoparticles

XRD was acquired using PAN analytical x, PERT PRO using ($\text{Cu K}\alpha$ radiation, $\lambda = 1.54060 \text{ \AA}$ at 40 kV and 40 mA. The surface morphology of the LDHs nanoparticles were picked up using (FE-SEM), Quanta 250 FEG (Field Emission Gun) equipped with energy dispersive X-ray spectrometer (EDX) for compositional analyses. (HR-TEM) (JEM-2100 Electron Microscope) has been done at 200 kV. The samples were mixed with ethyl alcohol by ultra-sonication, dropping them on copper grid, and then drying them in air. Evolution 300 UV–VIS double beam spectrophotometer was connected to monitor to record the changes of the dye absorbance during the course of reaction. The maximum absorbance wavelength of PN 4R

λ_{\max} (508 nm) all the results were checked using the same spectrophotometer and the same results were achieved [15]. The Fluorescence measurements were performed on Evolution 300 PC Spectro-fluoro photometer equipped with quartz cuvette of 1 cm path length and 2.5 nm slit width. Dispersive-Raman microscope & spectrometer ("Bruker Sentra"). Raman of the as-grown LDH samples were recorded by Dispersive Raman Microscope (Bruker Sentra). The apparatus was equipped with a diode Nd: YAG laser and wavelength of 532 nm. The experiments are in range of 0 to 2000 cm⁻¹.

3. Results and Discussion

3.A. Physico-Chemical Study

3.A.1. X-Ray Diffraction

Table 1 :Preparation, content and thermal treatment conditions with and without surfactants of Zn-Co/ TiO₂ LDH solids

Zn-Co LDH,	Treatment Zn-Co LDH, Temp, °C	Ti,	Prepared Ti by oleic or phosphate	Treatment Ti, Temp, °C	Ti/Zn-Co	Mixture Ti/Zn-Co Temp, °C	Index
-	-	1.0	phosphate	80	-	-	V
2.0	80	1.0	phosphate	80	0.50:1:1	80	XIII
2.0	80	1.0	phosphate	80	0.50:1:1	300	XIV
2.0	300	1.0	phosphate	300	0.50:1:1	80	XV
2.0	80	1.0	Phosphate with IHDTMA-Cl	80	0.50:1:1	300	XVI
2.0	80	1.0	Phosphate with DHDTMA-Cl	80	0.50:1:1	300	XVII
2.0	80	1.0	Phosphate With D Triton	80	0.50:1:1	300	XVIII
2.0	80	1.0	Phosphate With IH0.05M	80	0.50:1:1	300	XIX
2.0	80	1.0	Phosphate With IH0.03M	80	0.50:1:1	300	XX
2.0	80	1.0	Phosphate With IH0.01M	80	0.50:1:1	300	XXI

Zn-Co/TiO₂ LDH treated by phosphate co precipitation method of (I), (V), (XIII), (XIV), (XV), (XVI), (XVII) and (XVIII). The samples prepared by using phosphate shows in **Fig. 3** which refers more amorphous. It shows the XRD pattern of composites. Phosphate mesoporous titanium oxide at 80 °C match well with (JCPDS No. 00-002-0387) appears anatase titanium oxide (V) only at $2\theta = 25.3^\circ$ with other small diffraction peaks at 37.9° , 48.1° and 53.8° . After calcined at different temperatures, the crystalline size increases [16]. According to curve (XIII) the small diffraction peaks appears at 33° and 72.5° . After calcination at 300 °C (XIV) the diffraction peaks at $2\theta = 36.5^\circ$, 59.1° and 65° are appeared for (XV), It's diffraction peaks at $2\theta = 31.6^\circ$, 34.3° , 36.2° , 56.5° and 58.7° . The different diffraction peaks may lead to different activity for removal of organic pollutants. According to (XIV) composite was modified by cationic surfactant HDTMA-Cl with direct and indirect method and it was modified another surfactant triton x-100. This indicates that the surfactants show that there is no change in mineral composition, this implies that the modification does not affect the internal structure of the composite [17]. All XRD spectra (XVI), (XVII) and (XVIII), look similar by adding surfactants as shown in **Fig.3b**. Present in the XRD spectra are the peaks at 2θ of about 31.2° , 36.3° , 44.7° , 58.8° and 64.7° which indicate the presence of zinc-cobalt oxide and cobalt oxide structure. The absent of titanium is clearly observed, which may indicate the hiding of the signal by the support or the metal dispersion. But the closer analysis of the XRD spectra and JCPD base revealed that there are some observed peaks indicating that Co is present as Co₃O₄, Zn as ZnO, zinc-cobalt oxide as Zn Co₂O₄ which may affect of adsorption capacity of these solids.

3.A.2.HR-TEM

The HR-TEM images of (V) TiO₂ by precipitation method. The characterized particle size of (IV) is ordered and stable than (V). However, the mesoporous structure is completely destroyed for (V). **Fig. 4** show HR-TEM analysis for the composite consists of small Ti particles attached with the metal oxide (zinc and cobalt) nanoparticles. All the metal zinc and cobalt oxide particles were nearly cubic in composites and supported by X-ray. Images of composite prepared by phosphated mesoporous titanium oxide with the metal oxide (zinc and cobalt) nanoparticles and modified by surfactant (XIV), (XVI), (XVII) and (XVIII) show that the whisker-like morphology is clearly in (XVI), the modification has resulted in a loss of crystallinity so (XVI) is more stable and ordered than another.

3.A.3. AFM

The atomic force modulation AFM image nanoparticles are shown in **Fig. 5**. The AFM force modulation images were (50x50 nm) of the LDH (XIV) and (XVI). The 3D surface plot images show the preparation with phosphate mesoporous titanium oxide and the surface of the composite modified by surfactant (XVI) being well dispersed and smoother than the other composite (XIV). The arithmetic average of the absolute values of the surface height deviations measured from the mean plane (Ra) of composite (XVI) gives 6.6 nm smoother than without surfactant, which gives 8.5 nm. The root main square average of height deviation taken from the mean image data plane (Rq) is the value of the composite modified by surfactant

(XVI), which gives an 8.8 nm lower roughness than without surfactant, which gives 10.14 nm. Maximum profile peak height (Rp) with surfactant (XVI) gives 18.5 nm lower than without surfactant, which gives 19.32 nm as shown in **Table 2**.

Table 2: AFM force parameters of the LDH.

Composites	(Ra) / nm	(Rq) / nm	(Rp) / nm
(XIV)	08.53	10.14	19.3
(XVI)	06.69	08.18	18.5

3.A.4.Raman Spectroscopy Analysis

The efficiency of the formation of the zinc cobalt titanium oxide phase is shown by the Raman spectra of solid samples (XIV), (XV), and (XIII) in **Fig. 6**,

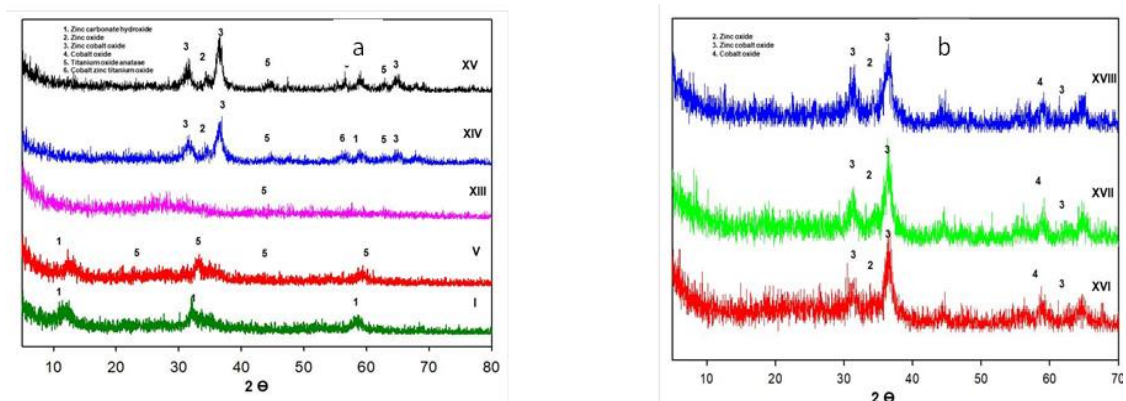


Fig. 3. Powder-XRD patterns of a. zinc-cobalt titanium oxide at different calcination temperature. b. zinc-cobalt titanium oxide with different surfactant

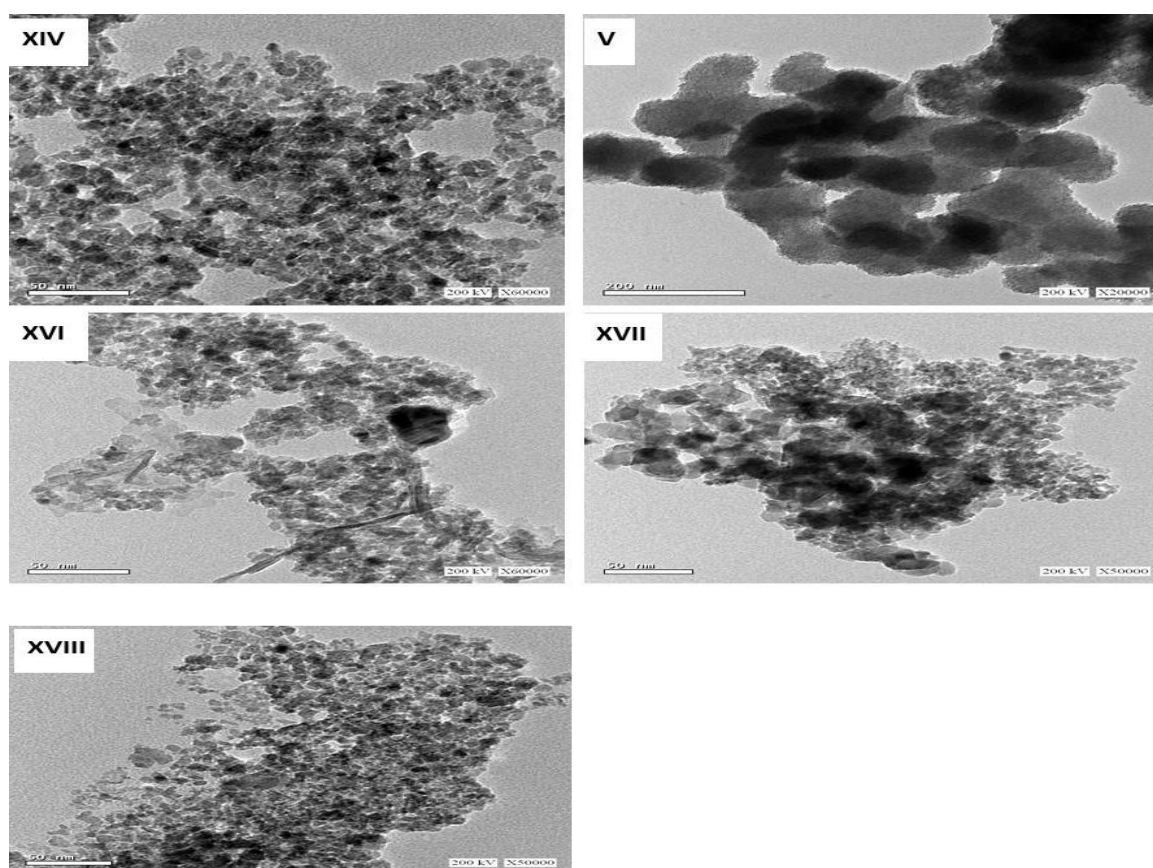


Fig. 4. HR-TEM of zinc-cobalt titanium oxide with different surfactants of solids XIV, V, XVI, XVII and XVIII

The quantitative depends on the difference in the intensity of the Raman bands characteristic of amorphous and crystalline phases on the temperature of the thermal treatment [18]. All figures show the main peaks for pure titanium oxide anatase at 155, 393, and 630 cm⁻¹ [19] induced by LDH TiO₂, only 396 and 617 cm⁻¹ in the Zn-Co LDH XIII composite. After calcination composite XIV and XV, the main peak of ZnO at 101 and 400 cm⁻¹ had almost appeared at these spots and appeared as Co₃O₄ at 507 and 609 cm⁻¹. The intensity of the Raman samples used in this study was linked to the surface roughness increasing simultaneously [20] so composite XIV and XV roughness are more supported with AFM. The appearance of six bands at about 101, 154, 266, 400, 609, and 705 cm⁻¹ can be attributed to characteristic vibration modes for titanium zinc cobalt at all spectral. It is important to note that the spectrum of ZnO is completely different from the spectrum of cobalt oxide. The mixture for zinc-cobalt only was not observed. All these observed differences may affect their behavior towards selectivity and activity in reactions.

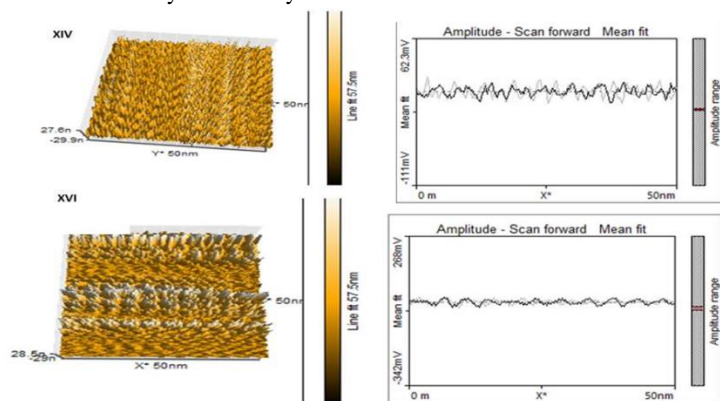


Fig. 5: AFM of Zn-Co/ TiO₂ LDH XIV and XVI.

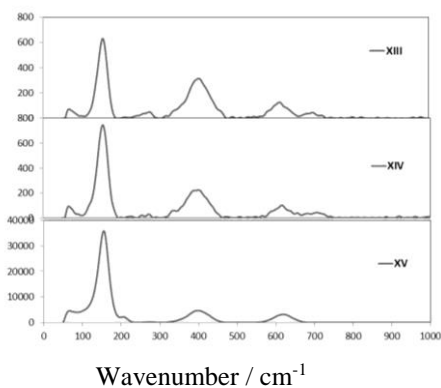


Fig. 6 : Raman spectra of XIII, XIV and XV composites prepared by phosphate

3.B. Application of Prepared Solids for Photocatalytic Degradation of Dyes

3.B.I. Effect of calcination temperature for Zn-Co / TiO₂ LDH treated with phosphate co precipitation method

Fig. 7 displayed Photo degradation of E124 dye at 20 ppm has been followed till 240 min on pure titanium oxide prepared by this catalyst on pure phosphate titanium oxide represent V, Ti- Zn Co LDH XIII, XII and XV. The dye solution was agitated for 15 min in dark in order to achieve the adsorption and desorption equilibrium between the dye and the catalyst material. After the addition of catalyst photocatalytic degradation for XIV is more active which gives removal 50% than another. Furthermore, photodegradation of dyes can be estimated by first order kinetics equation in which the rate constant (k) can be calculated from the slopes are 0.0024, -0.002, -0.0038 and -0.0013 min⁻¹, respectively for V, XIII, XIV and XV composite.

So, this composite modified by surfactant as shown in Fig. 7 due to lower activity than composite which prepared by hydrothermal method. The composite for the preparation of phosphate mesoporous titanium oxide at different calcination compositions is shown in Fig. 8. the photo degradation efficiency of the composites XIV is more active than the other, which gives 50%. As a result, the removal percent of composite XIV < XIII < XV phosphate titanium oxide is un-stable and it is modified by surfactant.

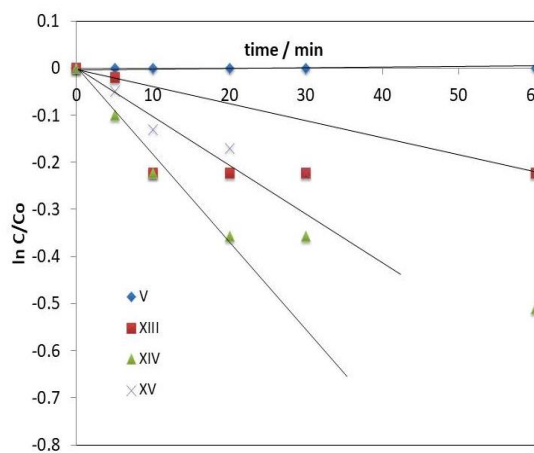


Fig. 7. Photodegradation kinetics of E124 dye at different calcination temperature with Zn- Co/ TiO₂ LDH.

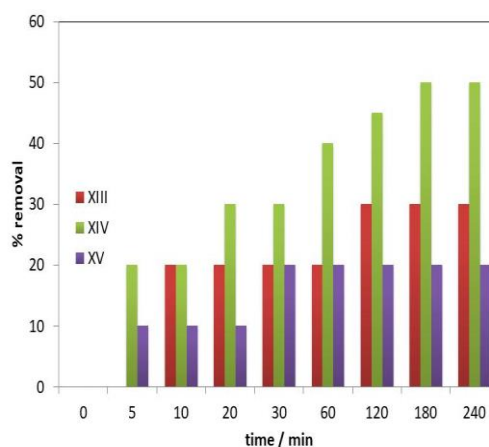


Fig. 8. Removal percent Photodegradation of E124 dye at different calcination temperature by different methods for preparation.

The plot of $\ln \frac{c}{c_0}$ versus time gave straight lines as shown in **Fig. 9a** with composite XIV (without surfactant), XVI (composite with HDTMA-Cl prepared by indirect method), XVII (composite with HDTMA-Cl prepared by direct method), and XVIII (composite with triton X-100 prepared by direct method) for E124 dye at 20 ppm, respectively. This indicates first-order kinetics concerning [21]. The rate constants show that the dye was rapidly degraded at 0.5 g/L of composites and gave -0.0038, -0.0046, -0.0079, and -0.1739, respectively, with composite XIV, XVIII, XVII, and XVI. It is important to note that composite XVI, which was prepared by the indirect method, has higher degradation efficiency than other prepared by direct method.

The removal percent for degradation reached 100% efficiency at 15 min in the dark before irradiation with composite XVI as shown in **Fig. 9b**. Therefore, the complete removal of color in this composite modified by surfactant prepared by indirect methods is due to the presence of bicarbonate and nitrate groups, which have main roles in the disappearance of dye color. So, the degradation percent in the descending order was as follows: XVI, XVII, XIV and XVIII.

3.B. III. Effect of concentration of HDTMA-Cl surfactant

As shown in **Fig. 10**, by increasing the concentration of surfactant by 0.1, 0.3, and 0.5 M for XXI, XX, and XIX, the degradation efficiency for the composite prepared by the phosphate precipitation method for titanium and then sonication mixing with zinc cobalt oxide increased to reach 100% with the composite XIX. According to this fitting, the maximum degradation efficiency is as follows: XIX > XXI > XX.

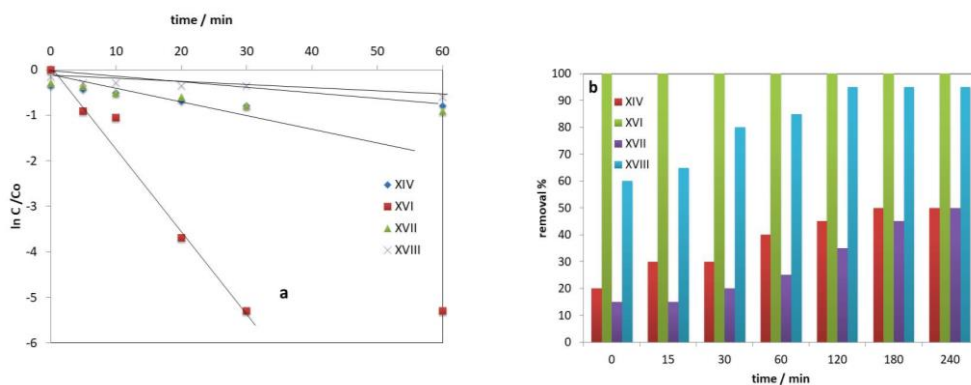


Fig. 9. Photodegradation of E124 dye by UV-visible spectra and removal percent for composite with different surfactants (a and b).

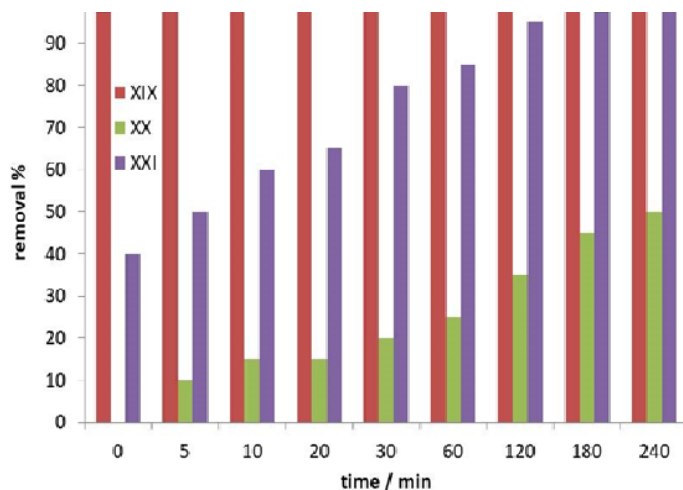


Fig. 10. Photodegradation of E124 dye by UV-visible spectra and removal percent for composite with different concentration of surfactant.

3.B. IV. Effect of concentration of E124 dye (adsorption and photo degradation)

The equilibrium of E124 adsorbed onto composite XIX was determined by performing adsorption and photo tests on 0.5 g/L XIX with flasks containing 100 ml of E124 solutions with different initial concentrations of 50, 70, and 100 ppm for 4.0 hours. Then the mixtures were analyzed using a UV-vis spectrophotometer at 508 nm. The adsorbed amount of E124 at equilibrium, q , which represented adsorption capacity, was calculated from the following equation:

$$q = \frac{(C_0 - C)}{W} V \text{ and removal\% as efficiency \%} = \frac{C_0 - C}{C_0} \times 100 \quad [22]$$

where C_0 and C are the initial and equilibrium concentrations of E124 dye in aqueous solution, respectively. V is the volume of dye solution, and W is the mass of the adsorbent. **Fig. 11a** shows the adsorption process, while **Fig. 11b** shows photo degradation. When using 20 ppm of E124 dye, the removal percent becomes 100% before irradiation. Therefore, using a higher concentration of dye, 50, 70, and 100 ppm, the photodegradation process becomes more degradation efficient than adsorption, which gives 60, 57, and 40% after 240 min, compared to 60, 50, and 27% with the adsorption process. The adsorption of E124 dye was also recorded at 50, 70, and 100 ppm at room temperature. **Fig. 12a** and **b** show the adsorption of Freundlich and Langmuir plots, respectively. In both cases, linear plots were obtained. The influence of concentration was studied by taking 100 mL of E124 dye and 0.5 g/L of adsorbent at room temperature.

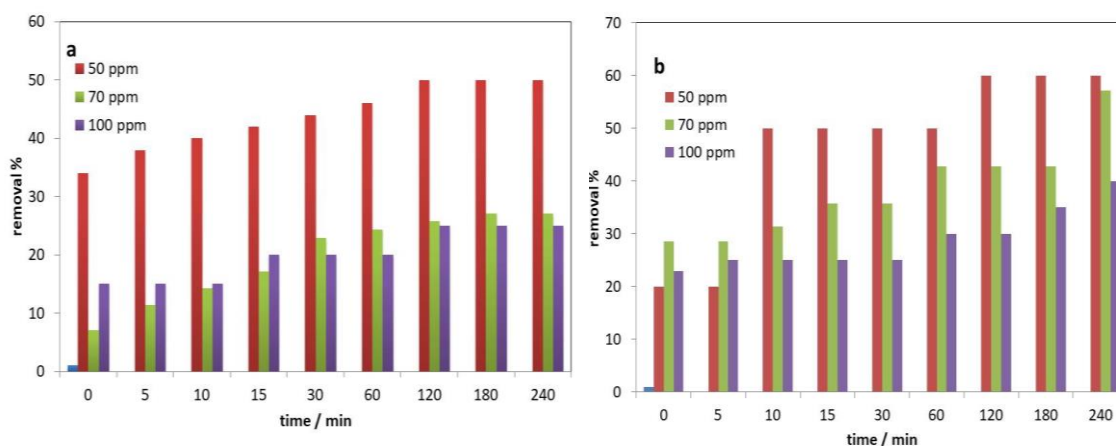


Fig. 11 a: Adsorption process and b: Photo degradation of E124 dye with different concentration.

As is obvious, the adsorption capacity (q) was increased with an upsurge in the strength of E124 dye by all concentrations; the elevated adsorption capability was displayed. The initial dye concentration is important as it expresses the adsorption process on the composite and thus provides an insight about the properties of the composite and the nature of interactions between adsorbent and adsorbate. The Langmuir and Freundlich adsorption isotherms are the two most frequently used models to explain the surface characteristics of the adsorbents, adsorbent affinity, and sorption mechanism. The Langmuir adsorption isotherm explains the assumption of monolayer adsorption: if the active sites are covered once by the adsorbate, then no adsorption will happen thereafter because of the comparable energy of all the active sites. The Freundlich adsorption isotherms, as shown in **Fig. 12b**, explain the multilayer and heterogeneous adsorption on the surface of an adsorbate. Furthermore, the kinetics model on the adsorption of E124 dye was highlighted using pseudo-first order and pseudo-second order kinetics as depicted in Eqs. Respectively.

$$\text{Log}(q_e - q_t) = \log q_e - \frac{k_1}{2.303} t \quad \text{and} \quad \frac{t}{q_e} = \frac{1}{k_2 q_e^2} + \frac{t}{q_e}$$

Pseudo-first-order kinetics described the process of diffusion, while pseudo-second order kinetics described the sorption capability of the adsorbent. The adsorption kinetics for the E124 dye adsorption was computed by applying the pseudo-first and pseudo-second-order kinetics (**Fig. 12a, b**). High R^2 values and a random distribution of the data for all the concentrations were found to be well fitted to pseudo-first-order kinetics. **Fig. 12a** indicates the linear pseudo-first order kinetics and residual plots. The Freundlich model fits the experimental statistics well, and the numerical value of the correlation coefficient of the Freundlich isotherm is higher than that of the Langmuir isotherm, indicating multilayer adsorption of E124 dye on the composite. Furthermore, the regular residual data derived from the Freundlich isotherm is well distributed compared to the Langmuir isotherm. The Langmuir and Freundlich adsorption isotherms can be articulated through Eqs. [23-26].

$$\frac{c_e}{q_e} = \frac{c_e}{q_m} + \frac{1}{k_l q_m} \quad \text{and} \quad \ln q_e = \ln k_f + \frac{1}{n} \ln c_e$$

The values and magnitude of $1/n$ indicate the adsorption favorability. If $1/n = 1$, the adsorption is irreversible, $1/n < 1$ the process is favorable, and if $1/n > 1$, the process is not favorable. By means of these current studies, the value of $1/n$ for the composite, which is less than 1, verifies the promising adsorption of E124 dye on the composite.

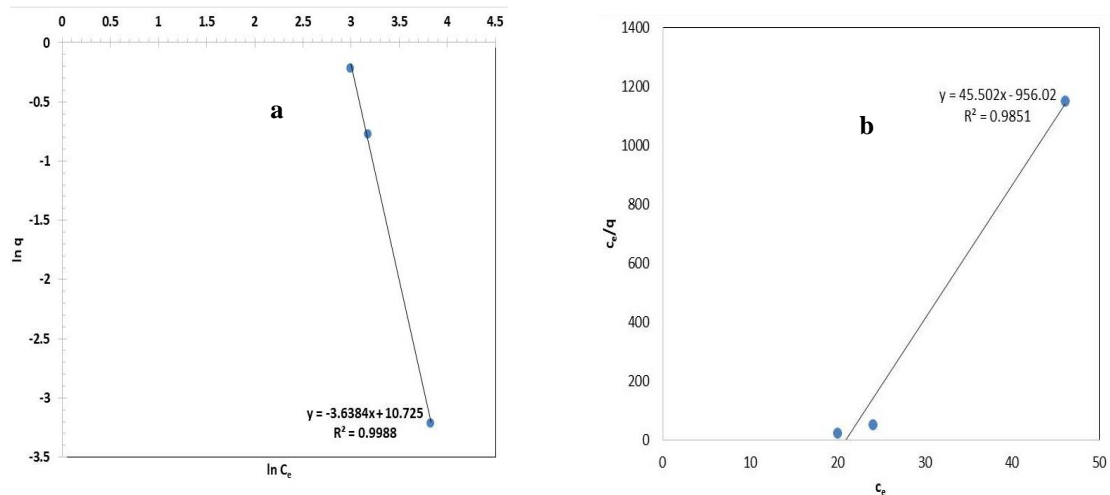


Fig. 12a: Freundlich and **b :** Langmuir adsorption isotherm for E124 dye at room temperature; amount of adsorbent = 0.5 g/L; time = one hour.

4. Conclusion

Binary LDH containing zinc and cobalt was successfully synthesized by co-precipitation of the metal salt at pH = 10. Modification of the samples occurred by doping of surfactants by direct and in direct method. XRD confirmed the formation of a pure cubic LDH nano-composite crystalline phase at 300° C and revealed that there is no effect on the structure of the composite. HR-TEM showed that whisker-like morphology and modification show in a loss of crystallinity. The highest activity for degradation of E124 dye.

The degradation reaction of the dye was carried out using LDH and UV-visible. The data observed as according to calcination temperature photodegradation of dye followed by first order kinetics and the most active sample is XIV with removal % reached to 50%. By modification of composite by in direct method with surfactant, the removal % reached to 100% efficiency at 15 min in the dark, and the most active one is XVI sample. The increasing the concentration of surfactant with in direct method, the efficiency of photodegradation increases, and the most active one is XIX. Study the effect of concentration of dye on the composite XIX by adsorption and photodegradation process, the results indicates that the efficiency reached to 60,57 and 40 % with concentration 50,70 and 100 ppm with photodegradation, while with adsorption reached to 60,50 and 27% .The adsorption kinetics well be fitted to pseudo first order kinetics and followed the Freundlich adsorption model.

Conflicts of interest

“There are no conflicts to declare”.

Acknowledgment

The authors would like to acknowledge the Faculty of Women for Art, Science, and Education, Ain Shams University, and the central lab at Egyptian Petroleum Research Institute for their great support in this research.

References

- [1] Shivaraj, P., et al., Recent advances in non-metals doped TiO₂ nanostructured photocatalysts for visible-light driven hydrogen production, CO₂ reduction and air purification, *International Journal of Hydroge Energy*, 2019, 44(26); pp. 1-18.
- [2] Dongjie, C., et al., Photocatalytic degradation of organic pollutants using TiO₂-based photocatalysts, A review. *Journal of Cleaner Production*, 2020, 268, 121725.
- [3] Eduardo, P., et al., TiO₂ Photocatalyzed Degradation of the Azo Dye Disperse Red 1
- [4] in Aqueous Micellar Environments, *Photochemistry and Photobiology*, 2021, 97: pp. 40–46.
- [5] Bin, N., et al., Mesoporous Titanium Dioxide: Synthesis and Applications in Photocatalysis, *Energy and Biology, Materials*, 2018, 11(10): 1910. pp. 1-23.
- [6] Zhou, W., et al., Mesoporous TiO₂: Preparation, doping, and as a composite for photocatalysis, *Chem. Cat. Chem.*, 2013, 5, pp. 885–894
- [7] Alberto, E. G., et al., Preparation and characterization of phosphate-modified mesoporous TiO₂ incorporated in a silica matrix and their photocatalytic properties in the photodegradation of Congo red, *Frontiers in materials science*, 2017, 11: pp. 250-261.
- [8] Qi, K., et al., A review on TiO₂-based Z-scheme photocatalysts. *Chinese Journal of Catalysis*, 2017, 38(12); pp. 1936-1955.

- [9] Abd-Ellatif, W.R., et al., Efficient photodegradation of E124 dye using two dimensional Zn-Co Technology & Innovation, 2022, 27, 102393.
- [10] Safa, G., et al., Modification of Clay Minerals by Surfactant Agents: Structure, Properties, and New Applications. Surfactants, Fundamental Concept and Emerging Perspectives, 2023,110317.
- [11] Raimondo, G., et al., Kinetic effects of cationic surfactants on the photocatalytic degradation of anionic dyes in aqueous TiO₂ dispersions, New Journal of Chemistry, 2023, 47: pp. 392-401.
- [12] Naef, A.A., Removal of heavy metal ions from wastewater: a comprehensive and critical review, npj Clean Water, 2021,4.
- [13] Teshale, A., et al., Textile Industry Effluent Treatment Techniques, Hindawi Journal of Chemistry, 2021, pp. 1-14.
- [14] Sharma, P., et al., Challenges in Effluents Treatment Containing Dyes, Advances Research Textile Engineering, 2022, 7(2), 1075.
- [15] Singh, A, et al., Biological remediation technologies for dyes and heavy metals in wastewater treatment: new insight, Bioresour. Technology. 2022a, 343:126154.
- [16] Beninca, C., et al., Degradation of an Azo Dye (Ponceau 4R) and Treatment of Wastewater from a Food Industry by Ozonation. Ozone-Science & Engineering, 2013,35(4): pp. 295-301.
- [17] Yu, J.C., et al., Synthesis and characterization of phosphated mesoporous titanium dioxide with high photocatalytic activity. Chemistry of Materials, 2003, 15(11): pp. 2280-2286.
- [18] Kaolinite, H.-C.M.J., Properties and Characterization of HDTMA-Cl Modified Jordanian Kaolinite and Its Use in Removal of Aniline from Aqueous Solution, Chemistry, 2014,3(10).
- [19] Alekseeva, I., et al., Features of the phase transformations in titanium-containing zinc aluminosilicate glasses doped with cobalt oxide. Glass Physics and Chemistry, 2013, 39(2): pp. 113-123.
- [20] Bøckman, O., et al., Raman spectroscopy of cemented cobalt on zinc substrates. Hydrometallurgy, 2000,55(1):pp.93-105.
- [21] Ekoi, E.J., et al., Characterisation of titanium oxide layers using Raman spectroscopy and optical profilometry: Influence of oxide properties. Results in Physics, 2019, 12: pp.1574-1585.
- [22] Hellna, T., et al., Characterization and Kinetic Study of Methylene Blue Photocatalytic on ZnO/ZSM-5, Indonesian Journal of Chemical Research, 2023,11 (2), pp.156-162.
- [23] Mizaj, S.S., et al., Photocatalytic degradation of organic dyes using reduced graphene oxide (rGO), Scientific Reports, 2024, 14:3608 pp. 1-14.
- [24] Mohamed, H.H., Kinetics and Adsorption Isotherm Studies of Methylene Blue Photodegradation Under UV Irradiation Using reduced Graphene Oxide- TiO Nanocomposite in Different Wastewaters Effluents, Egyptian Journal of Aquatic Biology & Fisheries, 2019, 23(1). pp. 253 -263.
- [25] Amina, K., et al., Photocatalytic Degradation Studies of Organic Dyes over Novel Cu/Ni Loaded Reduced Graphene Oxide Hybrid Nanocomposite: Adsorption, Kinetics and Thermodynamic Studies, Molecules ,2023, 28(18): 6474.
- [26] Mohamed H. H., et al., Characterization and photodegradation of methylene blue dye using bio-synthesized cerium oxide nanoparticles with Spirulina platensis extract, Discover Applied Sciences. 2024, 6:94.
- [27] Maria-Anna G., et al., Photodegradation of Rhodamine B and Phenol Using TiO₂/SiO₂ Composite Nanoparticles: A Comparative Study. Water, 2023, 15, 2773.